

## Expression Pattern of G Protein-Coupled Receptor 30 in LacZ Reporter Mice

Jörg Isensee, Luca Meoli, Valeria Zazzu, Christoph Nabzdyk, Henning Witt, Dian Soewarto, Karin Effertz, Helmut Fuchs, Valérie Gailus-Durner, Dirk Busch, Thure Adler, Martin Hrabé de Angelis, Markus Irgang, Christiane Otto, and Patricia Ruiz Noppinger

Center for Cardiovascular Research and Berlin Institute for Gender in Medicine (J.I., L.M., V.Z., C.N., H.W., D.S., K.E., M.I., P.R.N.), Charité Universitätsmedizin, 10115 Berlin, Germany; German Mouse Clinic (H.F., V.G.-D., T.A., M.H.d.A.), Institute of Experimental Genetics, Helmholtz Zentrum München, German Research Center for Environmental Health, 85764 Munich/Neuherberg, Germany; Institute for Medical Microbiology, Immunology, and Hygiene (D.B., T.A.), Technische Universität München, 81675 München, Germany; Department of Experimental Genetics (M.H.d.A.), Center of Life and Food Sciences Weihenstephan, Technische Universität München, 85354 Freising, Germany; and Therapeutic Research Group Women's Healthcare (C.O.), Bayer Schering Pharma AG, 13353 Berlin, Germany

Multiple reports implicated the function of G protein-coupled receptor (GPR)-30 with nongenomic effects of estrogen, suggesting that GPR30 might be a G-protein coupled estrogen receptor. However, the findings are controversial and the expression pattern of GPR30 on a cell type level as well as its function *in vivo* remains unclear. Therefore, the objective of this study was to identify cell types that express Gpr30 *in vivo* by analyzing a mutant mouse model that harbors a lacZ reporter (Gpr30-lacZ) in the Gpr30 locus leading to a partial deletion of the Gpr30 coding sequence. Using this strategy, we identified the following cell types expressing Gpr30: 1) an endothelial cell subpopulation in small arterial vessels of multiple tissues, 2) smooth muscle cells and pericytes in the brain, 3) gastric chief cells in the stomach, 4) neuronal subpopulations in the cortex as well as the polymorph layer of the dentate gyrus, 5) cell populations in the intermediate and anterior lobe of the pituitary gland, and 6) in the medulla of the adrenal gland. In further experiments, we aimed to decipher the function of Gpr30 by analyzing the phenotype of Gpr30-lacZ mice. The body weight as well as fat mass was unchanged in Gpr30-lacZ mice, even if fed with a high-fat diet. Flow cytometric analysis revealed lower frequencies of T cells in both sexes of Gpr30-lacZ mice. Within the T-cell cluster, the amount of CD62L-expressing cells was clearly reduced, suggesting an impaired production of T cells in the thymus of Gpr30-lacZ mice. (**Endocrinology 150: 1722–1730, 2009**)

The human G protein-coupled receptor (GPR)-30, initially cloned in 1996–1997 from different human sources by several groups (1–5), has partial similarity to the angiotensin and chemokine receptors (1, 3).

Multiple reports suggested that GPR30 might be a G protein-coupled estrogen receptor mediating nongenomic estradiol effects. A well-known nongenomic effect of estrogen, which is essential for uterine epithelial cell proliferation as well as ductal elongation and endbud growth in the mammary gland, is the transactivation of the epidermal growth factor receptor (EGFR)

(6–8). Filardo *et al.* (9, 10) proposed in initial reports that GPR30 mediates the estrogen-induced phosphorylation of ERK1/2 via the transactivation of the EGFR in breast cancer cell lines lacking classical nuclear estrogen receptors (ERs). In these studies it remained unclear whether GPR30 binds estradiol in a direct manner or acted downstream of another receptor. Indeed, considerable evidence was provided that classical ERs associate with the plasma membrane and transmit nongenomic estrogen signaling (11), including the transactivation of the EGFR pathway (12). Subsequently two groups claimed in 2005 that GPR30

ISSN Print 0013-7227 ISSN Online 1945-7170  
Printed in U.S.A.  
Copyright © 2009 by The Endocrine Society  
doi: 10.1210/en.2008-1488 Received October 23, 2008. Accepted December 8, 2008.  
First Published Online December 18, 2008

Abbreviations: DIG, Digoxigenin; EGFR, epidermal growth factor receptor; ER, estrogen receptor; ES, embryonic stem; FACS, fluorescent-activated cell sorting; gal, galactosidase; GFAP, glial fibrillary acidic protein; GPR, G protein-coupled receptor; ORF, open reading frame; PECAM-1, platelet/endothelial cell adhesion molecule 1; SMC, smooth muscle cell.

For editorial see page 1563

directly binds estradiol and mediates rapid nongenomic signaling (13, 14). Estradiol stimulation of GPR30-transfected COS-7 cells induced the release of intracellular calcium and the synthesis of phosphatidylinositol 3,4,5-trisphosphate in the nucleus (14). However, the number of reports that question the function of GPR30 as a transmembrane ER is growing (15, 16). In a recent publication, saturable and specific binding of radioactive estradiol was observed only to ER $\alpha$  but not GPR30 (16). Estradiol stimulation of cells expressing GPR30 had no impact on intracellular cAMP levels or calcium release (16).

Beside the controversy regarding the ligand, the expression pattern of GPR30 on a cell type level as well as its function *in vivo* is unclear. Because Gpr30 mRNA and protein expression was found to be regulated by gonadotrophic hormones in granulosa and theca cells of hamster ovaries, a possible role of Gpr30 for the reproductive system was suggested (17, 18). Supporting a potential function of Gpr30 in the hypothalamic-pituitary-gonadal axis, Gpr30 expression colocalized with oxytocin-positive neurons in the rat hypothalamus (19, 20). However, the GPR30-selective agonist G1 (21, 22) did not stimulate estrogenic effects in the uterus or mammary gland of mice (16). Gpr30-deficient mouse models are fertile and exhibit normal reproductive functions (23).

A recent study by Wang *et al.* (24) implicated the function of Gpr30 in estrogen-induced thymic atrophy. Studies with ER $\alpha$ -, ER $\beta$ -, and Gpr30-deficient mice showed that ER $\alpha$  and Gpr30 are partially responsible for the reduction in thymus size, whereas ER $\beta$  is not relevant (24–26). ER $\alpha$  mediated exclusively the early developmental blockage of thymocytes, whereas Gpr30 was indispensable for thymocyte apoptosis (24). Subsequently Martensson *et al.* (27) reported that female Gpr30-deficient mice had hyperglycemia and impaired glucose tolerance, reduced body growth, increased blood pressure, and reduced serum IGF-I levels. These metabolic consequences of Gpr30 deficiency were associated with a decreased insulin expression and release *in vivo* as well as *in vitro* from isolated pancreatic islets.

However, a prerequisite for the analysis of the physiological role of Gpr30 is a detailed knowledge about the tissue distribution at the cell type level. Several studies investigated the expression of Gpr30 by real-time PCR (27), ribonuclease protection assays (23), or Northern (1–3) or Western blotting (15, 17) in various tissues. However, the findings are inconsistent and the applied methods do not provide information about the relevant cell types. Furthermore, the rat brain has been investigated in more detailed studies with immunohistochemistry as well as *in situ* hybridization (20, 28). Nevertheless, the major drawback of these studies is the lack of critical experiments clearly confirming the specificity of used antibodies and probes.

Therefore, the objective of this study was to identify cell types that express Gpr30 *in vivo* by analyzing a mutant mouse model that harbors a LacZ reporter (Gpr30-lacZ) in the Gpr30 locus leading to a partial deletion of the Gpr30 coding sequence. Using this approach, we provide a cellular basis for the function of Gpr30 *in vivo*. In further experiments, we aimed to decipher the function of Gpr30 by analyzing the phenotype of Gpr30-lacZ mice.

## Materials and Methods

### Gpr30-lacZ mice

Gpr30-lacZ mice (Deltagen, T181) were generated by homologous recombination in embryonic stem (ES) cells (Fig. 1A). ES cells derived from the 129Sv strain were transfected with the linearized targeting construct. G418-resistant clones were analyzed by Southern blotting using a probe that hybridized outside of the 5' homology arm of the targeting vector and long, range PCR. One recombinant clone harboring the targeted allele was used for the generation of chimeric mice by blastocyst injection. Chimeric mice were bred to C57BL/6J females. Heterozygous offspring were backcrossed to the C57BL/6J parental strain for six generations. Mice were maintained on a 12-h light, 12-h dark cycle and provided with food and water *ad libitum*. All animal procedures are complied with the German animal welfare law with the permission of the District Government of Berlin.

### Genotyping of Gpr30-lacZ mice

Tail tips were digested in tail lysis buffer [300 mM sodium acetate; 5 mM EDTA; 1% Triton X-100; 10.0 mM Tris-HCl, (pH 8.3), 750  $\mu$ g/ml proteinase K] overnight at 55 C. The PCR (1.5 mM Mg<sup>2+</sup>, 200  $\mu$ M deoxynucleotide triphosphates, 200 nM primer, 0.05 U *Taq*) was performed with 1:10 diluted tail DNA as template. The endogenous allele was amplified using primers G1 (ACCTGTCTCGAAGCTCATCCAGGT-GAG) and G2 (GGTGGAGATCTACCTAGGTCCCGTG); the targeted allele was amplified using primers G1 and G3 (GGGGATCGATC-CGTCTGTAAGTCT).

### Southern blotting

Probe sequences were amplified from genomic liver DNA using primers P1 (CCCGAATTCGTGCCATCTCAGGTAGGAGC) and P2 (CCCGAATTCAGAGCTGAGGTGCTTTCC) for the 5' probe, P3 (CCCGAATTCCTTCTGCGTACTCTCCTATGTACC) and P4 (CCCGAATTCGCTGCCAAGTCCACTAAACC) for the 3' probe, and P5 (CCCGAATTCACGTCTCTTTCCAACACTGC) and P6 (CCCGAATTCAGTAGTCGCATCCATGGCTTCC) for the internal probe. Digoxigenin (DIG) labeling was performed with the PCR DIG probe synthesis kit (Roche Applied Science, Mannheim, Germany). For Southern blotting, 5  $\mu$ g genomic liver DNA were digested with 100 U of *EcoRI*, *BamHI*, or *HindIII* overnight. Digested DNA was separated by gel electrophoresis (0.8% agarose in Tris-borate EDTA buffer) at 30 V overnight. The DNA was denatured in the gel, transferred onto a nylon membrane (Roche), and UV cross-linked to the membrane. The hybridization was performed according to standard protocols in DIG Easy Hyb buffer (Roche Applied Science) at 46.5 C overnight. Probe-target hybrids were visualized by chemiluminescence (Roche).

### Real-time PCR

Total RNA was isolated using Trizol (Invitrogen, Carlsbad, CA). Approximately 500 ng total RNA was reverse transcribed using the Multi-Scribe RT kit (Applied Biosystems, Foster City, CA) with random hexamers. Real-time PCRs were performed in triplicate using SYBR-Green I master mix (Applied Biosystems). Normalization and error propagation were calculated as described (29). Relative quantities were normalized to hypoxanthine-guanine phosphoribosyltransferase. Specific primers were designed for Gpr30 (ACCTGTCTCGAAGCTCATCCAGGT-GAG, GGTGGAGATCTACCTAGGTCCCGTG) and LacZ (GTGCA-CATGCTTTACATGTGTTT, GTGGCCATATTATCATCGTGTTT).

### X-galactosidase (gal) reporter assay

Tissues were fixed in fixative (PBS with 2% paraformaldehyde, 2 mM MgCl<sub>2</sub>) on ice for 1–4 h and rinsed in PBS with 2 mM MgCl<sub>2</sub>. For whole-mount staining, tissues were incubated in X-gal reaction buffer (PBS with 1 mg/ml X-gal, 10 mM potassium ferrocyanide, 10 mM potassium ferricyanide, 2 mM MgCl<sub>2</sub>, 0.02% Nonidet P-40 substitute, 0.01% sodium deoxycholate) for 3–5 h at 37 C. For frozen sections, the

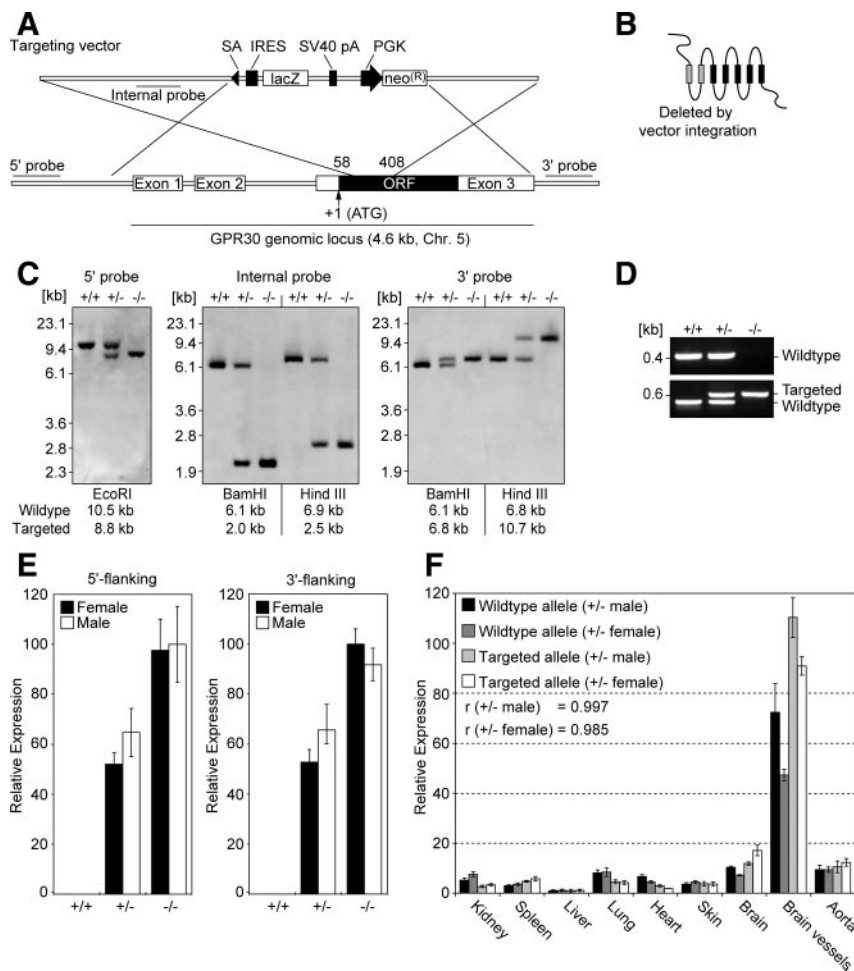


**FIG. 1.** Gene targeting strategy and molecular characteristics of *Gpr30-lacZ* mice. **A**, Exon 3 encoding the ORF of the *Gpr30* gene has been disrupted by insertion of a cassette containing a splice acceptor (SA), an internal ribosomal entry site (IRES), a  $\beta$ -galactosidase gene (*lacZ*), a Simian virus 40 (SV40) polyadenylation site, and a neomycin-resistance gene (*neo<sup>R</sup>*) driven by a phosphoglycerate kinase promoter (PGK). **B**, The insertion deleted 349 bp of the ORF encoding the first two transmembrane domains and the first intra- and extracellular loop, respectively. **C**, Genomic liver DNA of wild-type, heterozygous, and homozygous *Gpr30-lacZ* mice was digested and analyzed by Southern hybridization probing with DIG-labeled probes that hybridize outside and adjacent to the 5' and 3' construct arms and in the targeting vector (internal probe). The detected fragments had the expected size (indicated below the blots) for all probes. **D**, Genotyping of *Gpr30-lacZ* mice. The wild-type fragment (433 bp) was absent in homozygous mutant mice, whereas a larger fragment indicating the targeted allele (618 bp) was amplified exclusively in *Gpr30-lacZ* mice. **E**, Real-time PCR quantification of sequences flanking the cassette (5' and 3' flanking) using brain cDNA of homozygous and heterozygous *Gpr30-lacZ* mice and wild-type controls. The cassette is spliced to the 5' region of exon 3 in the mutated transcript. In addition, a fusion transcript of the *neo<sup>R</sup>* gene and the remaining 3' region of exon 3 was detected in *Gpr30-lacZ* mice. **F**, Quantification of the wild-type and targeted allele in various tissues of one male and one female heterozygous *Gpr30-lacZ* mouse by real-time PCR. The expression of wild-type and targeted allele correlated significantly (Pearson correlation coefficient  $r > 0.9$ ).

tissues were submerged in 30% sucrose in PBS at 4 C overnight. Tissues were embedded and snap frozen on dry ice. Frozen blocks were cut in 5- to 25- $\mu$ m-thick cryostat sections and mounted on slides. For X-gal staining, frozen sections were postfixed for 10 min at 4 C, rinsed for 20 min at room temperature, and transferred into X-gal reaction buffer for 1–5 h. Sections were counterstained with Nuclear Fast Red (Sigma-Aldrich, Munich, Germany), dehydrated quickly, and coverslipped in Permount mounting medium (Fisher Scientific, Pittsburgh, PA).

**Immunohistochemistry**

The sections were blocked in serum blocking buffer (2% goat serum, 1% BSA, 0.1% fish skin gelatin, 0.05% Tween 20) for 30 min and incubated with the primary antibody diluted in PBS with 1% BSA at 4 C

overnight. Primary antibodies were directed against glial fibrillary acidic protein (GFAP; rabbit polyclonal, 1:1000; Abcam, Cambridge, MA), platelet/endothelial cell adhesion molecule 1 (PECAM-1; rat monoclonal, MEC 7.46, 1:250; GeneTex, Irvine, CA), and  $\alpha$ -smooth muscle cell (SMC) actin conjugated with Cy3 (mouse monoclonal, 1:500; Sigma). Subsequently the sections were rinsed in PBS and incubated with Alexa488- or Alexa568-conjugated secondary antibodies (Molecular Probes, Eugene, OR) and counterstained with 4',6'-diamino-2-phenylindole. The green fluorescent Nissl staining was performed according to the manufacturer's instructions (Molecular Probes).

**Mammalian cell culture and transfections**

HeLa cells were cultured in DMEM with 10% fetal bovine serum and antibiotics. Transfections were performed with FuGENE 6 reagent (Roche Applied Science) according to the manufacturers' instructions.

**Cloning**

A construct encoding human GPR30 tagged with enhanced green fluorescent protein was kindly provided by Professor Eric Prossnitz (University of New Mexico, Albuquerque, NM). GPR30 was amplified by PCR and subcloned into pcDNA3.1(+) for native expression without tag.

**Western blotting**

Cells were lysed in 10-cm plates 48 h after transfection in 450  $\mu$ l lysis buffer [100 mM Tris-HCl (pH 8), 2% sodium dodecyl sulfate, 3.2 M urea] supplemented with 64 mM dithiothreitol, 0.5 mM phenylmethylsulfonyl fluoride, and 1 $\times$  complete protease inhibitor mixture (Roche). Cell lysates were sonicated and denatured at 37 C for 20 min, separated by SDS-PAGE, and transferred to a polyvinylidene difluoride membrane (Hybond-P; Amersham, Amersham, UK). After blocking in 125 mM Tris-HCl (pH 8), 625 mM NaCl, 0.1% Tween 20 with 5% nonfat milk, membranes were incubated with the primary antibody (rabbit anti-GPR30 third extracellular domain, MBL, LS-A4271, diluted 1:500) at 4 C overnight. The immune complexes were detected by an enhanced chemiluminescence detection system (Amersham).

**High-fat diet, magnetic resonance imaging, and glucose tolerance testing**

Six-month-old mice were placed on a high-fat diet (BCMIPS, London, UK; 60 kcal percent fat, 21 kcal percent carbohydrates, 19 kcal percent protein; 5.2 kcal/g) or control diet (10 kcal percent fat, 71 kcal percent carbohydrates, 18 kcal percent protein; 3.8 kcal/g) for 6 months ( $n = 10$ /group). Body weights were recorded twice per week between 1000 and 2400 h. Total body fat and lean mass of mice was assessed after 2 and 6 months using an EchoMRI system (Echo Medical Systems, Houston, TX). Before glucose tolerance testing, animals were fasted for 15 h. Subsequently glucose solution (0.2 g/ml in 0.9% NaCl) was injected ip (1 g glucose per kilogram body weight). Glucose levels were measured in tail blood drops at 0, 15, 30, 60, 90, and 120 min.

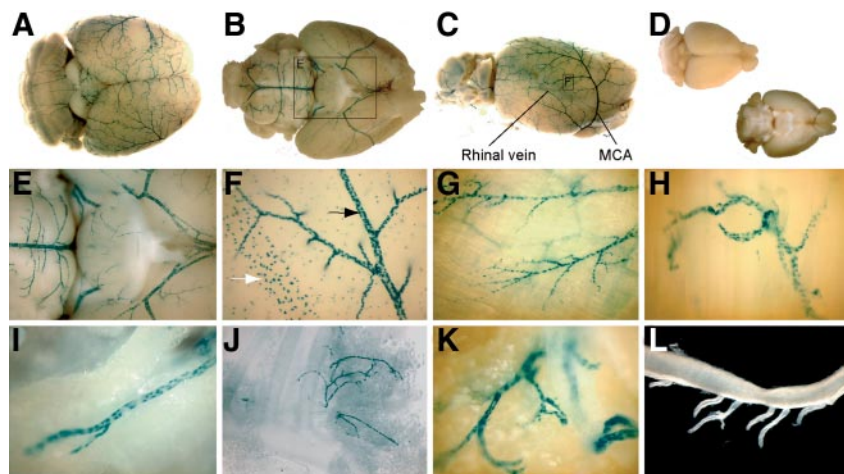


**FIG. 2.** Whole-mount X-gal staining indicating vessel-associated expression of the LacZ reporter in *Gpr30-lacZ* mice. LacZ-positive cells were found in all vessels covering the brain (A–F; D shows the wild-type control). The circle of Willis (E) and a major branch of the middle cerebral artery (*black arrow* in F) and the rhinal vein (*white arrow* in F) are shown enlarged. Arterial vessels contained more LacZ-positive cells compared with venous vessels. Furthermore, LacZ-positive cells were found in smaller vessels of diverse tissues including the peritoneum (G), hamstring muscle (H), perimetrial fat (I), mesenteric fat (J), and outer layer of the aorta (K). LacZ-positive cells were absent in the aorta (L). MCA, middle cerebral artery.

### Analysis of peripheral blood leukocytes by flow cytometry

Peripheral blood leukocytes were collected after resuspension of the cell pellet in 500  $\mu$ l  $\text{NH}_4\text{Cl}$ -Tris solution to lyse the red blood cells, filtrated through nylon net, and placed into 96-well plates. Cells were washed with  $\text{NH}_4\text{Cl}$ -Tris [ $\text{H}_2\text{O}$ ,  $\text{NH}_4\text{Cl}$ , Tris-HCl (pH 7.5)] and fluorescent-activated cell sorting (FACS) buffer [PBS, 0.5% BSA, 0.02% sodium azide (pH 7.45)], respectively, and incubated for 20 min with Fc block (BD PharMingen, Heidelberg, Germany). Cells were stained with conjugated monoclonal antibodies (BD PharMingen, Caltag Laboratories GmbH, Hamburg, Germany) and propidium iodide (20  $\mu$ g/ml) and washed with FACS buffer repeatedly. Single-color controls were run parallel to the samples on the same plate. Samples were acquired automatically from 96-well plates with a High Throughput Screening on a LSRII flow cytometer (Becton Dickinson, San Diego, CA) until a number of 30,000 living CD45<sup>+</sup> cells was reached for each well and were analyzed using FlowJo (TreeStar, Inc.; Ashland, OR).

## Results

### Molecular characteristics of *Gpr30-lacZ* mice

To investigate the expression and function of *Gpr30* *in vivo*, we used a mouse model (*Gpr30-lacZ*) generated by homologous recombination in ES cells targeting exon 3 that encodes the open reading frame (ORF) of *Gpr30* (Fig. 1A). The insertion replaced 349 bp of the ORF encoding amino acids 20–136 of *Gpr30*, accounting for the first two transmembrane domains as well as the first intra- and extracellular loop (Fig. 1B). The integration of the cassette into the mouse genome was verified by Southern blotting with probes that hybridize 5' and 3' to the homology arms and in the cassette (internal probe) (Fig. 1C). The detected fragments had always the expected size, confirming a successful homologous recombination event.

For genotyping reactions, forward primers located upstream or in the cassette were combined with a gene-specific primer binding downstream of the integration site. The wild-type fragment (433 bp) was absent in homozygous *Gpr30-lacZ* mice,

whereas a larger fragment indicating the targeted allele (618 bp) was specifically amplified in the *Gpr30-lacZ* mice (Fig. 1D).

Real-time PCR quantification of sequences flanking the cassette in brain cDNA samples verified the fusion of the lacZ transcript to the 5'-part of exon 3 (Fig. 1E). In addition, a fusion transcript of the neoR gene and the remaining 3'-region of exon 3 was detected in the mutant mice (Fig. 1E). The expression of this transcript starts at the phosphoglycerate kinase promoter and leads to overexpression of a truncated *Gpr30* transcript in *Gpr30-lacZ* mice as determined by real-time PCR (data not shown). However, the expression of a truncated protein is unlikely due to stop codons in all three reading frames terminating the neomycin resistance and due to a nonsense reading frame of the remaining transcript.

To assure that the integration of the reporter cassette in the *Gpr30* locus did not affect the endogenous promoter activity, we quantified the expression of the wild-type as well as the targeted allele in various tissues by real-time PCR (Fig. 1F). The results revealed that the expression of the wild-type and the targeted allele correlated significantly (Pearson correlation coefficient  $r > 0.98$ ). Highest expression was detected in isolated brain vessels; lowest expression was detected in the liver.

Unfortunately, we were unable to rule out residual expression of a truncated protein. Consistent with other studies (23, 24), our efforts to detect the murine *Gpr30* protein by Western blotting or immunohistochemistry using three different commercially available antibodies directed against the N-terminal, first extracellular, and third extracellular domain as well as an antiserum detecting the C-terminal domain (14) failed so far (for details, refer to the supplemental data published on The Endocrine Society's Journals Online web site at <http://endo.endojournals.org>). Two of these antibodies (third extracellular domain, C-terminal domain) detected ectopically expressed human GPR30 with a C-terminal enhanced green fluorescent protein tag in transiently transfected HeLa cells (supplemental Fig. 1A). As reported previously (14, 16), tagged and untagged GPR30 seemed to be retained in the endoplasmic reticulum and was not processed to the membrane in HeLa cells. The antibody directed against the third extracellular domain also detected human GPR30 by Western blotting using cell lysates from GPR30 transfected HeLa cells (supplemental Fig. 1B).

### Tissue distribution of LacZ expression

The finding that the expression of the LacZ reporter and the wild-type *Gpr30* correlated at transcript level encouraged us to track *Gpr30*-positive cells *in vivo* by X-gal staining. To ensure specific staining, wild-type littermates were always included as negative controls. Because the employed LacZ reporter included a nuclear localization signal, we expected predominant nuclear staining in case of specific signals. For all staining procedures,

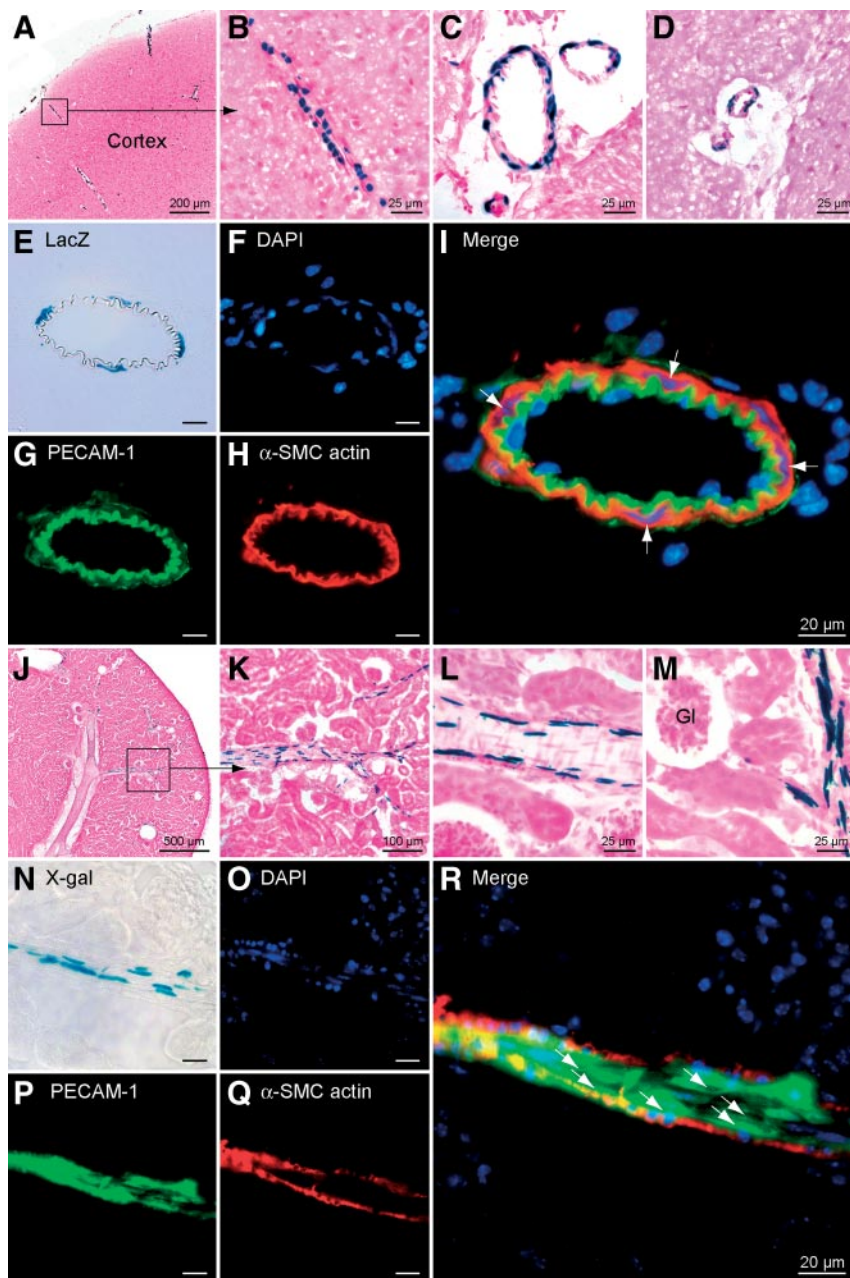


**FIG. 3.** X-gal staining followed by immunohistochemistry in frozen sections from brain (A–I) and kidney (J–R). LacZ-positive cells were present in all brain vessels (A–D) and colocalized with  $\alpha$ -SMC actin (red signal, E–I). In contrast, LacZ-positive cells in the kidney were restricted to specialized vascular beds (J–M) and were a PECAM-1-positive endothelial subpopulation (green signal, P). Cell nuclei were visualized with 4',6'-diamino-2-phenylindole (DAPI; blue signal, F, O). LacZ-positive nuclei are indicated by arrows in the merged images. Gl, Glomerulus.

8-wk-old male and female heterozygote mice were used. A summary of the LacZ expression data in diverse tissues from Gpr30-lacZ mice is depicted in supplemental Table 1.

Consistent with our real-time PCR data, multiple LacZ-positive cells were found in surface vessels of the brain (Fig. 2, A–F). Interestingly, arterial vessels including the middle cerebral artery (black arrow in Fig. 2F), and its rostral and caudal branches were found to contain more LacZ-positive cells compared with venous vessels (e.g. the caudal rhinal vein, white arrow in Fig. 2F). Moreover, LacZ-positive cells were found ubiquitously in arterial blood vessels of many tissues including the peritoneum (Fig. 2G),

skeletal muscle (Fig. 2H), and fat depots (Fig. 2, I–J). However, the expression of the reporter appeared to be restricted to cells of special vascular beds. For instance, the large vessels, such as the thoracic and abdominal aorta (Fig. 2L) and its adjacent branching vessels like the carotid arteries, intercostal arteries, renal arteries, and superior mesenteric arteries were negative for LacZ-positive cells. In contrast, small arterioles of the vasa vasorum in the outer layer of the aorta (Fig. 2K) as well as the final branches of the mesenteric arteries (Fig. 2J) contained a large number of LacZ-positive cells.

In the next step, we aimed to unravel the cell type(s) expressing the LacZ reporter in frozen sections. In the brain, vessel-associated LacZ-positive cells were ubiquitously present and appeared to be attached either outside or inserted into the basal lamina (Fig. 3, A–D). We demonstrated that LacZ-positive cells colocalized with  $\alpha$ -SMC actin and not with PECAM-1 (CD31), which is a marker for endothelial cells (Fig. 3, E–I). Therefore, LacZ-positive cells were smooth muscle cells and pericytes in the brain.

However, in other tissues we assumed that LacZ-positive cells might be an endothelial subpopulation because the cells appeared to be attached to the luminal site of the vessel. For instance, in the kidney, LacZ-positive cells were specifically located in smaller arteries (i.e. arcuate and interlobular arteries) as well as afferent arterioles supplying the glomeruli (Fig. 3, J–M). In contrast to cells detected in the brain, LacZ-positive cells in the kidney were located at the luminal site of the vessel and colocalized with PECAM-1 but not  $\alpha$ -SMC actin (Fig. 3, N–R). Further studies revealed that LacZ-positive vessel-associated cells were present in multiple organs, but restricted to only a few and small arteries/arterioles in most tissues.

Previous RT-PCR results indicated prominent expression of Gpr30 in the stomach and pancreas of wild-type mice (supplemental Fig. 2).

Indeed, we detected LacZ-positive cells located at the base of fundic glands (Fig. 4, A–D). Within this area, gastric chief (zymogenic) cells and enteroendocrine cells are the most prominent cell populations. However, only chief cells are exclusively present in fundic glands and absent in cardiac or pyloric glands known to express enteroendocrine cells. We therefore assumed that LacZ-positive cells in fundic glands are gastric chief cells.

In the context of the endocrine system, we analyzed the expression pattern of the LacZ reporter in several glands as well as the gonads. LacZ expression was located in blood vessels in most of these tissues (i.e. thyroid gland, harderian gland, coagulating

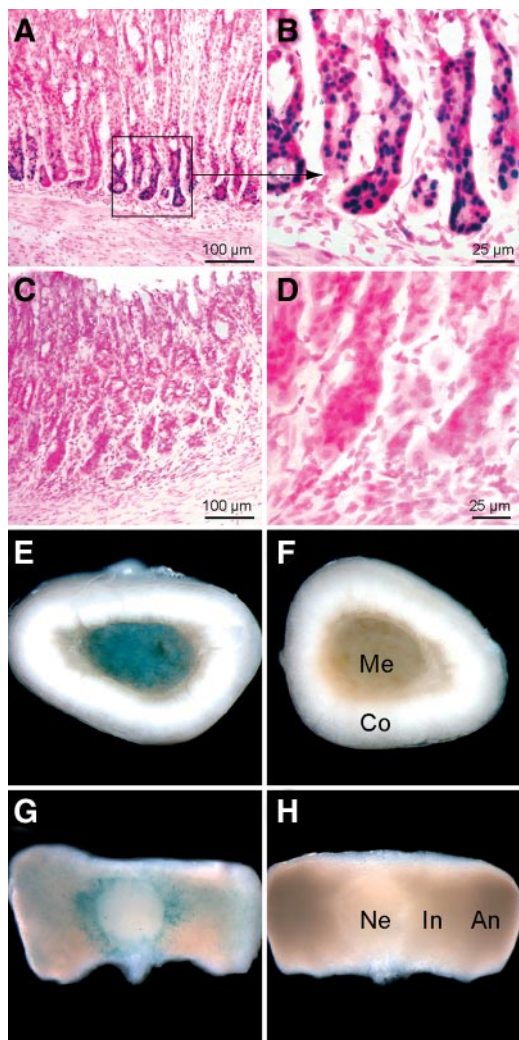


**FIG. 4.** X-gal staining of frozen sections from the stomach of heterozygous Gpr30-lacZ mice (A and B) and wild-type controls (C and D). LacZ-positive gastric chief cells were found in the gastric fundus (blue nuclei in A and B). Whole-mount X-gal staining of the adrenal (E and F) and pituitary gland (G and H). LacZ-positive cells were located in the medulla of the adrenal gland (E) and the intermediate and anterior lobe of the pituitary gland (G). In corresponding wild-type controls (F and H), the LacZ-activity was absent. Me, Medulla; Co, cortex; Ne, neurohypophysis; In, intermediate lobe; An, anterior lobe.

gland, and testis). In addition, LacZ-positive cells were found in the medulla of the adrenal gland (Fig. 4, E and F) and the intermediate and anterior lobe of the pituitary gland (Fig. 4, G and H). In contrast to other locations, the LacZ staining was not nuclear but scattered all over the cell body in the adrenal and pituitary gland.

Because nonvessel-associated LacZ-positive cells were present in cortical areas of the brain, we analyzed coronal sections of whole brains in detail. We found two distinct brain structures containing these cells (Fig. 5). The first structure that contained LacZ-positive cells was the polymorph layer of the dentate gyrus, which is a part of the hippocampal formation (Fig. 5, A–C). The second region was located in the lateral part of the cerebral cortex, in which LacZ-positive cells were mainly located in the second layer (Fig. 5, A and D). In subsequent studies, we demonstrated that these cells are in fact neuronal subpopulations. The X-gal staining colocalized with fluorescent Nissel

staining used as a general marker for neuronal cells and not with the astrocyte marker GFAP, PECAM-1, or  $\alpha$ -SMC actin in the dentate gyrus (Fig. 5, E and F) and cortex (Fig. 5, J–N).

### Phenotypic assessment of Gpr30-lacZ mice

To gain insight into the function of Gpr30 *in vivo*, we undertook considerable efforts to identify phenotypes in Gpr30-lacZ mice. At the age of weaning, Gpr30-LacZ mice were found at the expected Mendelian ratio. The body weight as well as lean and fat mass determined by magnetic resonance imaging was not different in homozygous Gpr30-lacZ mice compared with wild-type littermates (supplemental Fig. 3). Due to the prominent expression of Gpr30 in the stomach, pancreas, and vessel system, we decided to challenge potential phenotypes by feeding the mice with a high-fat diet containing 60% of kcal from fat compared with a control diet with 10% kcal from fat. However, wild-type and homozygous Gpr30-lacZ mice gained the same weight and no differences regarding the body composition were observed (supplemental Fig. 3). Furthermore, glucose tolerance testing did not reveal reproducible differences between Gpr30-lacZ mice and wild-type siblings fed with the control or high fat diet, respectively (supplemental Fig. 4).

In parallel, a primary phenotype screen was performed at the German Mouse Clinic [<http://www.mouseclinic.de> (30)] that included the following methods: behavior (open field, acoustic startle, prepulse inhibition); cardiovascular (blood pressure, heart weight, echocardiography); clinical chemistry (simplified ip glucose tolerance test, clinical chemical analysis, hematology); dysmorphology (dual-energy x-ray absorptiometry); energy metabolism (calorimetry); eye (eye size, ophthalmoscopy, slit lamp); immunology and allergy (FACS analysis of peripheral blood cells, immune globulin concentrations); lung function (plethysmography); neurology (mod. SHIRPA<sup>1</sup> protocol, grip strength, rotarod); nociception (hot plate); pathology (macro- and microscopic analysis); steroid metabolism (dehydroepiandrosterone, testosterone); and molecular phenotyping (cDNA microarrays).

A significant difference in Gpr30-lacZ mice when compared with wild-type siblings was found in the immunology screen. Under baseline conditions, the proportion of T cells in peripheral blood leukocytes (CD45<sup>+</sup>) was decreased in Gpr30-lacZ mice (Table 1). The fraction of CD4<sup>+</sup> cells was reduced by 24.8% in females and 30.2% in males. The number of CD8<sup>+</sup> cells was lowered by 20.6% in females and 28.2% in males. Moreover, the proportion of cells expressing CD62L within the T cell compartment was significantly lower in Gpr30-lacZ mice (59.0% in females, 44.9% in males). These results have been confirmed with a second bleeding in an independent group. Full reports of the immunology screen are shown in supplemental Table 1. Parts of the primary phenotype assessment was performed following the EMPReSSslim protocols (31). The data set will be available on the EuroPhenome web page (<http://www.europhenome.org/>).

<sup>1</sup>SmithKline Beecham Pharmaceuticals; Harwell, MRC Mouse Genome Centre and Mammalian Genetics Unit; Imperial College School of Medicine at Saint Mary's; Royal London Hospital, Saint Bartholomew's and the Royal London School of Medicine; Phenotype Assessment.

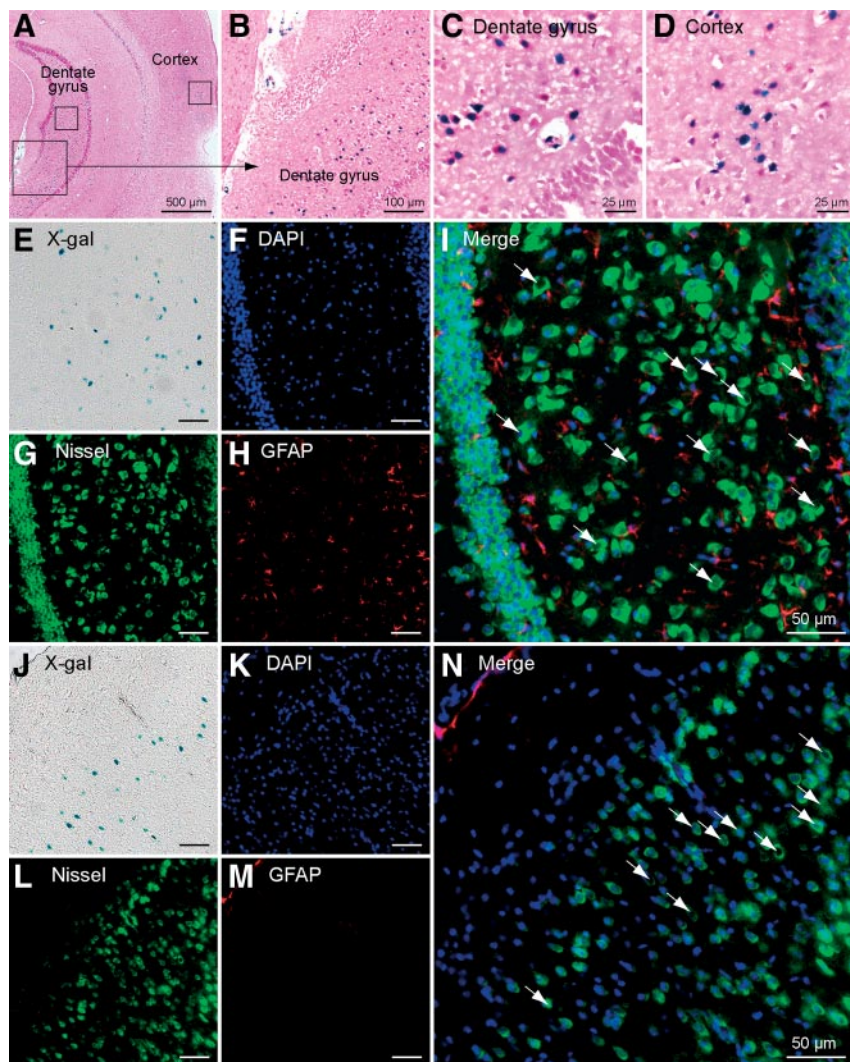


**FIG. 5.** X-gal staining followed by immunohistochemistry and Nissel staining of frozen sections from the brain. LacZ-positive cells were present in the polymorphic layer of the dentate gyrus (A–C) and the cortex (A and D). LacZ-positive cells colocalized with the Nissel staining that indicates neuronal cells (green signal) in the dentate gyrus (E–I) and the cortex (J–N). No colocalization was detected with the astrocyte marker GFAP (red signal). LacZ-positive nuclei are indicated by white arrows in the merged images.

## Discussion

Expression of Gpr30 has been reported for numerous murine and human tissues, suggesting a ubiquitous expression of the receptor at low levels (23). However, the cellular basis of the expression profile remained unknown due to a lack of specific methods that enable the detection of Gpr30 protein within tissues. To tackle this question, we analyzed the expression of a LacZ reporter in Gpr30-lacZ mice and characterized the identified cell types by colocalization of LacZ along with cell type-specific markers. This approach is especially useful if low expression levels are assumed because the LacZ assay allows remarkable signal amplification.

Using this strategy, we identified the following Gpr30-expressing cell populations: 1) an endothelial cell subpopulation in small arterial vessels of multiple tissues (*e.g.* kidney, heart, peritoneum, genital tract), 2) smooth muscle cells and pericytes in the brain, 3) gastric chief cells in the stomach, 4) neuronal subpopulations in layer II of the cortex as well as in

the polymorph layer of the dentate gyrus, and 5) cell populations in the intermediate lobe and adenohypophysis of the pituitary gland, and 6) chromaffin cells in the medulla of adrenal glands.

The expression profile of LacZ resembled the expression profile of the wild-type transcript as shown by real-time PCR. A ubiquitous expression of Gpr30 mRNA at low levels might correspond to LacZ-positive vessel-associated cells found in Gpr30-lacZ mice. Published data obtained by ribonuclease protection assays revealed prominent expression of Gpr30 mRNA in the stomach, followed by the adrenal gland (23). These findings are consistent with our results describing LacZ-positive chief cells in the gastric fundus and chromaffin cells in the medulla of the adrenal glands. In agreement with published data (23, 27), we did not detect Gpr30 mRNA as well as LacZ reporter activity in the liver and thymus. We therefore concluded that Gpr30-lacZ mice represent a valid Gpr30 reporter model.

Two studies reported that Gpr30 is expressed by oxytocin-positive neurons in the paraventricular and supraoptic nuclei of the rat hypothalamus (19, 20). The expression of Gpr30 was determined by immunohistochemistry using an antiserum directed against the C-terminal domain (14) of the human GPR30 (19, 20) and *in situ* hybridization (20). In contrast to these reports, we did not observe LacZ-positive neurons in the paraventricular and supraoptic nuclei of Gpr30-lacZ mice. In the hypothalamus, all identified LacZ-positive cells were associated to vessels and colocalized with  $\alpha$ -SMC

actin. In addition to oxytocin-positive neurons (20), granulosa cells of preantral follicles as well as mammary and uterine epithelial cells were found to express Gpr30 in an estrous cycle-dependent manner (17, 18). Conversely, in our study granulosa, mammary, and uterine epithelial cells were negative for LacZ expression. However, we found LacZ-positive cells located in blood vessels, which may explain the expression of Gpr30 mRNA in these tissues. As demonstrated already in other Gpr30 mutant mouse models (23, 24, 27), Gpr30-lacZ mice were fertile and showed no reproductive abnormalities. These findings exclude a direct function of Gpr30 in the reproductive system of mice.

Matsuda *et al.* (28) recently reported the expression of GPR30 in pyramidal cells of the hippocampal regions CA1–3 and granule cells of the dentate gyrus detected by *in situ* hybridization and immunohistochemistry. In contrast, we found lacZ-positive neurons only in the polymorphic layer of the dentate gyrus. This layer contains many interneurons and axons of granule cells that

**TABLE 1.** Frequencies of T cell subsets [percent of viable CD45+ leukocytes] and CD62L+ cells within the T cell compartment of homozygous Gpr30-lacZ mice and wild-type littermates (n = 10 per group)

Parameter	First bleeding			Second bleeding		
	Gpr30-lacZ	Wild type	P value	Gpr30-lacZ	Wild type	P value
Females						
CD3+	21.5 ± 0.9	26.6 ± 1.6	< 0.05	18.7 ± 0.9	24.0 ± 1.7	< 0.05
CD3e+/CD4+	9.7 ± 0.5	12.9 ± 1.1	< 0.05	8.5 ± 0.4	11.6 ± 1.0	< 0.05
CD3e+/CD8a+	8.5 ± 0.4	10.7 ± 0.7	< 0.05	7.4 ± 0.4	9.9 ± 0.7	< 0.01
CD4+/CD62L+	16.8 ± 4.8	40.1 ± 6.4	< 0.01	25.6 ± 5.2	58.9 ± 6.0	< 0.001
CD8a+/CD62L+	19.0 ± 5.6	47.4 ± 7.2	< 0.01	29.8 ± 5.6	66.3 ± 6.8	< 0.001
Males						
CD3+	13.6 ± 1.3	18.7 ± 1.0	< 0.01	12.3 ± 1.0	17.2 ± 1.0	< 0.01
CD3e+/CD4+	6.0 ± 0.6	8.6 ± 0.6	< 0.01	5.1 ± 0.5	7.43 ± 0.6	< 0.01
CD3e+/CD8a+	5.6 ± 0.5	7.8 ± 0.5	< 0.01	5.9 ± 0.5	8.06 ± 0.4	< 0.01
CD4+/CD62L+	22.6 ± 7.1	43.4 ± 7.1	n.s.	16.8 ± 2.8	42.6 ± 7.9	< 0.01
CD8a+/CD62L+	28.2 ± 7.1	48.6 ± 7.2	n.s.	24.2 ± 3.4	50.1 ± 8.1	< 0.05

Results of two independent bleedings are shown. Values are given as means ± SEM.

pass the polymorphic layer. We therefore assume that these cells are interneurons and not granule cells.

Several reasons need to be considered to explain the inconsistent expression pattern of LacZ compared with previous reports. We and others (23, 24, 27) were unable to show the absence of the protein in Gpr30 mutant mice. This underlines the difficulty to detect Gpr30 protein in tissues, probably due to low expression of Gpr30, its lipophilic properties as a seven-transmembrane receptor, and the lack of specific antibodies detecting mouse Gpr30. However, cell type-specific differences in the activity of the internal ribosomal entry site element initiating LacZ translation may also influence the results masking low expression of Gpr30.

In line with our findings that LacZ reporter expression is prominent in small arterial vessels of multiple tissues, an elevated blood pressure and an increased media to lumen ratio of second-order mesenteric arteries was described in 9-month-old female Gpr30-deficient mice (27). Moreover, expression of GPR30 mRNA was recently reported for human internal mammary arteries and saphenous veins (32). Our own attempts to detect changes in blood pressure failed, probably because the mice were of younger age.

In contradiction to recently published data by Martensson *et al.* (27), we did not detect significant genotype-related differences concerning the body weight or glucose metabolism in female Gpr30-lacZ mice. Feeding of Gpr30-lacZ mice with a high-fat diet induced the same weight gain as in wild-type control siblings. Our results are in line with another Gpr30-deficient model on a pure C57BL/6 background that did not show a body weight phenotype (23). Because the mice in the study of Martensson *et al.* were on a mixed background, and it remained unclear whether the control groups were littermates or C57BL/6 mice, strain-specific differences may have influenced the results.

Flow cytometric analysis of peripheral blood in the primary German Mouse Clinic Immunology Screen revealed statistically lower frequencies of T cells in Gpr30-lacZ mice compared with wild-type controls. Within the T cell cluster, the amount of CD62L expressing cells was clearly reduced. CD62L-expressing

T cells represent the naive T cell compartment newly produced in the thymus (33). The phenotype of Gpr30-lacZ mice might be explained by a lower rate of T cells produced in the thymus. A T cell phenotype has been already reported in a Gpr30-deficient mouse model by Wang *et al.* (24), whereas the authors suggested a function of Gpr30 for thymocyte apoptosis during estrogen-induced thymic atrophy. In agreement with our findings, the apoptosis rate in T-cell receptor  $\beta^{-low}$  double-positive (CD4+, CD8+) thymocytes was doubled in Gpr30-deficient mice when compared with wild-type controls. Therefore, the lower frequency of CD4+ and CD8+ T cells in the peripheral blood found here can be explained by pronounced apoptosis of these cells in the thymus. However, several lines of evidence question the role of estrogen in this process: 1) the T-cell phenotype is not sexually dimorphic in Gpr30-lacZ mice, 2) the finding that ER $\alpha$  deficiency is not sufficient to block estrogen-induced thymic atrophy completely is based on findings in hypomorphic ER $\alpha$ -mutant mice that express functional splicing variants (34), 3) the increased apoptosis rate in Gpr30-deficient mice may mask the effect of estrogen, and 4) a critical experiment involving the GPR30 agonist G1 could not be reproduced by others (16). Moreover, the T cell phenotype identified here and by Wang *et al.* might also be caused by a linkage of the mutation to genes from the 129 strain or the presence of the neomycin cassette. For both models, ES cells of the 129Sv background have been used and neomycin cassettes have not been removed from the Gpr30 locus. In contradiction to a direct function of Gpr30 in the thymus, Gpr30 mRNA expression (23) and LacZ-positive cells were absent in the thymus.

In summary, we expect that our findings concerning the LacZ expression in Gpr30-lacZ mice are important and provide a cellular basis for future studies of Gpr30-deficient mouse models. These studies, however, should be performed with mouse models on a pure genetic background that are devoid of resistance and reporter cassettes. Furthermore, the analysis of conditional knockouts will be necessary to dissect the functions of Gpr30 in different tissues.

## Acknowledgments

We thank Carola Geiler and Aydah Sabah for excellent technical assistance. We also thank the members of the German Mouse Clinic for comprehensive phenotyping of the Gpr30-deficient mice and fruitful discussions.

Address all correspondence and requests for reprints to: Professor Dr. Patricia Ruiz Noppinger, Center for Cardiovascular Research, Charité Universitätsmedizin Berlin, Hessische Strasse 3-4, 10115 Berlin, Germany. E-mail: patricia.ruiz@charite.de.

This work was supported by Nationales Genomforschungsnetz Deutschland Grants (01GR0430 (to H.F., V.G.-D., and M.H.d.A.) and 01GR0435 (to T.A. and D.B.)) from the Bundesministerium für Bildung und Forschung and European Union Grant LSHG-2006-037188 (German Mouse Clinic). J.I. was funded by the Research and Training Group 754 “Sex- and Gender-Specific Mechanisms in Myocardial Hypertrophy” (German Research Foundation). V.Z. and L.M. are fellows of the Marie Curie Program CARDIOVASC (MEST-CT-2005-020268).

Disclosure Summary: The authors have nothing to disclose.

## References

- Owman C, Blay P, Nilsson C, Lolait SJ 1996 Cloning of human cDNA encoding a novel heptahelix receptor expressed in Burkitt's lymphoma and widely distributed in brain and peripheral tissues. *Biochem Biophys Res Commun* 228:285–292
- Carmeci C, Thompson DA, Ring HZ, Francke U, Weigel RJ 1997 Identification of a gene (GPR30) with homology to the G-protein-coupled receptor superfamily associated with estrogen receptor expression in breast cancer. *Genomics* 45:607–617
- Feng Y, Gregor P 1997 Cloning of a novel member of the G protein-coupled receptor family related to peptide receptors. *Biochem Biophys Res Commun* 231:651–654
- Kvingedal AM, Smeland EB 1997 A novel putative G-protein-coupled receptor expressed in lung, heart and lymphoid tissue. *FEBS Lett* 407:59–62
- Takada Y, Kato C, Kondo S, Korenaga R, Ando J 1997 Cloning of cDNAs encoding G protein-coupled receptor expressed in human endothelial cells exposed to fluid shear stress. *Biochem Biophys Res Commun* 240:737–741
- Mukku VR, Stancel GM 1985 Regulation of epidermal growth factor receptor by estrogen. *J Biol Chem* 260:9820–9824
- Nelson KG, Takahashi T, Bossert NL, Walmer DK, McLachlan JA 1991 Epidermal growth factor replaces estrogen in the stimulation of female genital-tract growth and differentiation. *Proc Natl Acad Sci USA* 88:21–25
- Ankrapp DP, Bennett JM, Haslam SZ 1998 Role of epidermal growth factor in the acquisition of ovarian steroid hormone responsiveness in the normal mouse mammary gland. *J Cell Physiol* 174:251–260
- Filardo EJ, Quinn JA, Bland KI, Frackelton Jr AR 2000 Estrogen-induced activation of Erk-1 and Erk-2 requires the G protein-coupled receptor homolog, GPR30, and occurs via trans-activation of the epidermal growth factor receptor through release of HB-EGF. *Mol Endocrinol* 14:1649–1660
- Filardo EJ, Quinn JA, Frackelton Jr AR, Bland KI 2002 Estrogen action via the G protein-coupled receptor, GPR30: stimulation of adenylyl cyclase and cAMP-mediated attenuation of the epidermal growth factor receptor-to-MAPK signaling axis. *Mol Endocrinol* 16:70–84
- Hammes SR, Levin ER 2007 Extracellular steroid receptors: nature and actions. *Endocr Rev* 28:726–741
- Razandi M, Pedram A, Park ST, Levin ER 2003 Proximal events in signaling by plasma membrane estrogen receptors. *J Biol Chem* 278:2701–2712
- Thomas P, Pang Y, Filardo EJ, Dong J 2005 Identity of an estrogen membrane receptor coupled to a G protein in human breast cancer cells. *Endocrinology* 146:624–632
- Revankar CM, Cimino DF, Sklar LA, Arterburn JB, Prossnitz ER 2005 A transmembrane intracellular estrogen receptor mediates rapid cell signaling. *Science* 307:1625–1630
- Pedram A, Razandi M, Levin ER 2006 Nature of functional estrogen receptors at the plasma membrane. *Mol Endocrinol* 20:1996–2009
- Otto C, Rohde-Schulz B, Schwarz G, Fuchs I, Klewer M, Brittain D, Langer G, Bader B, Prelle K, Nubbemeyer R, Fritzsche KH 2008 GPR30 localizes to the endoplasmic reticulum and is not activated by estradiol. *Endocrinology* 19:19
- Wang C, Prossnitz ER, Roy SK 2007 Expression of G protein-coupled receptor 30 in the hamster ovary: differential regulation by gonadotropins and steroid hormones. *Endocrinology* 148:4853–4864
- Prossnitz ER, Arterburn JB, Smith HO, Oprea TI, Sklar LA, Hathaway HJ 2008 Estrogen signaling through the transmembrane G protein-coupled receptor GPR30. *Annu Rev Physiol* 70:165–190
- Brailoiu E, Dun SL, Brailoiu GC, Mizuo K, Sklar LA, Oprea TI, Prossnitz ER, Dun NJ 2007 Distribution and characterization of estrogen receptor G protein-coupled receptor 30 in the rat central nervous system. *J Endocrinol* 193:311–321
- Sakamoto H, Matsuda K, Hosokawa K, Nishi M, Morris JF, Prossnitz ER, Kawata M 2007 Expression of G protein-coupled receptor-30, a G protein-coupled membrane estrogen receptor, in oxytocin neurons of the rat paraventricular and supraoptic nuclei. *Endocrinology* 148:5842–5850
- Bologa CG, Revankar CM, Young SM, Edwards BS, Arterburn JB, Kiselyov AS, Parker MA, Tkachenko SE, Savchuck NP, Sklar LA, Oprea TI, Prossnitz ER 2006 Virtual and biomolecular screening converge on a selective agonist for GPR30. *Nat Chem Biol* 2:207–212
- Revankar CM, Mitchell HD, Field AS, Burai R, Corona C, Ramesh C, Sklar LA, Arterburn JB, Prossnitz ER 2007 Synthetic estrogen derivatives demonstrate the functionality of intracellular GPR30. *ACS Chem Biol* 2:536–544
- Otto C, Fuchs I, Kauselmann G, Kern H, Zevnik B, Andreasen P, Schwarz G, Altmann H, Klewer M, Schoor M, Vonk R, Fritzsche KH 2009 GPR30 does not mediate estrogenic responses in reproductive organs in mice. *Biol Reprod* 80:34–41
- Wang C, Dehghani B, Magrisso IJ, Rick EA, Bonhomme E, Cody DB, Elenich LA, Subramanian S, Murphy SJ, Kelly MJ, Rosenbaum JS, Vandenberg AA, Offner H 2008 GPR30 contributes to estrogen-induced thymic atrophy. *Mol Endocrinol* 22:636–648
- Staples JE, Gasiewicz TA, Fiore NC, Lubahn DB, Korach KS, Silverstone AE 1999 Estrogen receptor alpha is necessary in thymic development and estradiol-induced thymic alterations. *J Immunol* 163:4168–4174
- Erlundsson MC, Ohlsson C, Gustafsson JA, Carlsten H 2001 Role of oestrogen receptors  $\alpha$  and  $\beta$  in immune organ development and in oestrogen-mediated effects on thymus. *Immunology* 103:17–25
- Martensson UE, Salehi SA, Windahl S, Gomez MF, Sward K, Daszkiewicz-Nilsson J, Wendt A, Andersson N, Hellstrand P, Grande PO, Owman C, Rosen CJ, Adamo ML, Lundquist I, Rorsman P, Nilsson BO, Ohlsson C, Olde B, Leeb-Lundberg LM 2008 Deletion of the G protein-coupled receptor GPR30 impairs glucose tolerance, reduces bone growth, increases blood pressure, and eliminates estradiol-stimulated insulin release in female mice. *Endocrinology* 150:687–698
- Matsuda K, Sakamoto H, Mori H, Hosokawa K, Kawamura A, Itose M, Nishi M, Prossnitz ER, Kawata M 2008 Expression and intracellular distribution of the G protein-coupled receptor 30 in rat hippocampal formation. *Neurosci Lett* 441:94–99
- Vandesompele J, De Preter K, Pattyn F, Poppe B, Van Roy N, De Paepe A, Speleman F 2002 Accurate normalization of real-time quantitative RT-PCR data by geometric averaging of multiple internal control genes. *Genome Biol* 3:RESEARCH0034
- Gailus-Durner V, Fuchs H, Becker L, Bolle I, Brielmeier M, Calzada-Wack J, Elvert R, Ehrhardt N, Dalke C, Franz TJ, Grundner-Culemann E, Hammelbacher S, Hölter SM, Hölzlwimmer G, Horsch M, Javaheri A, Kalaydjiev S, Klempt M, Kling E, Kunder S, Lengger L, Lisse T, Mijalski T, Naton B, Pedersen V, et al. 2005 Introducing the German Mouse Clinic: open access platform for standardized phenotyping. *Nat Methods*:403–404
- Mallon AM, Blake A, Hancock JM 2008 EuroPhenome and EMPReSS: online mouse phenotyping resource. *Nucleic Acids Res* 36:D715–D718
- Haas E, Meyer MR, Schurr U, Bhattacharya I, Minotti R, Nguyen HH, Heigl A, Lachat M, Genoni M, Barton M 2007 Differential effects of 17 $\beta$ -estradiol on function and expression of estrogen receptor  $\alpha$ , estrogen receptor  $\beta$ , and GPR30 in arteries and veins of patients with atherosclerosis. *Hypertension* 49:1358–1363
- Blais ME, Brochu S, Giroux M, Belanger MP, Dulude G, Sekaly RP, Perreault C 2008 Why T cells of thymic versus extrathymic origin are functionally different. *J Immunol* 180:2299–2312
- Pendaries C, Darblade B, Rochaix P, Krust A, Chambon P, Korach KS, Bayard F, Arnal JF 2002 The AF-1 activation-function of ER $\alpha$  may be dispensable to mediate the effect of estradiol on endothelial NO production in mice. *Proc Natl Acad Sci USA* 99:2205–2210